IR Ultraspectral Remote Sensing –Efficient Physical-Statistical Non-linear Sounding Retrieval Algorithms

William Smith Sr[a,b], Stanislav Kireev[b], Elisabeth Weisz[a], Jian Yongxiao[b], Melissa Yesalusky[b], Allen Larar[c], and Henry Revercomb[b]

[a]University of Wisconsin-Madison, Madison WI, USA,
[b]Hampton University, Hampton VA, USA, [c]NASA Langley Research Center, Hampton VA, USA.

ABSTRACT

Two solutions to the radiative transfer equation are described for profiling the atmosphere using ultraspectral infrared radiance measurements. The sounding retrieval algorithms are fast non-linear physical-statistical algorithms. The first solution described, applied to ground-based ultraspectral radiance measurements, is a statistical matrix inverse solution of the radiative transfer equation where the optimal matrix inverse stability factor is chosen by trial and error as that value which minimizes the RMS difference between the retrieval calculated radiance spectrum and the observed radiance spectrum. The second solution, applied to satellite and aircraft ultraspectral radiance observation, is a fast non-linear "Physical Dual-Regression " method trained to produce accurate retrievals for both clear and cloudy sky conditions. The second method relies on using Eigenvector Regression (EOF) "Clear-trained" and "Cloud-trained" retrievals of: surface skin temperature, surface emissivity PC-scores, CO_2 concentration, cloud top altitude, effective cloud optical depth, and atmospheric temperature, moisture, and ozone profiles above the cloud and below thin or scattered cloud (i.e., cloud effective optical depth < 1.5 and a cloud induced temperature profile attenuation < 15 K. The "Clear-trained" regression is a relation relating a "clear sky equivalent" perturbed profile from a clouded radiance spectrum (e.g., an isothermal profile below an opague cloud cover) to the observed radiance spectrum. The "Cloud-trained" regression relates the true atmospheric profile, both above and below cloud level, to the observed radiance spectrum. Results from the application of both of these algorithms are presented in this paper.

Keywords: Ultra-spectral, hyper-spectral, satellites, meteorology, sounding, remote sensing

I. Algorithms

The sounding retrieval algorithms presented here are fast physical-statistical algorithms intended for the retrieval of atmospheric profiles from groundbased, aircraft, and satellite ultraspectral radiance observations[1] . For ground-based AERI[2,3] and ASSIST [4] ultraspectral radiance measurements the solution is a statistical matrix inverse solution of the radiative transfer equation. The satellite and aircraft ultraspectral observation sounding retrieval method uses a "Physical Dual-Regression " method trained solutions to produce accurate retrievals for both clear and cloudy sky conditions.

Ground-based Sounding Retrieval Methodology: The ground-based radiance sounding retrieval algorithm developed has the form:

$$q_{ret} = q_o + (r_m - r_o)C$$

where the vector q_{ret} represents the retrieved atmospheric profiles of temperature and water vapor, C is a statistical regression coefficient matrix computed from atmospheric profile and associated computed radiance spectra deviations from an initial profile q_o and r_o, respectively. The statistical regression coefficient matrix, C, is given by,

$$C = (R'^{T}R' + \lambda E^{T}E)^{-1}R'^{T}Q'$$

where Q and R are climatological ensembles of atmospheric profiles and associated computed radiance spectra, ( )' represents a deviation from the initial conditions q_o and r_o, $E^{T}E$ is a statistical covariance of spectral radiance noise, and λ is a scaler determined by trial and error as that value which minimizes the RMS difference between the retrieval calculated radiance spectrum and the observed radiance spectrum.

Satellite and Aircraft Sounding Retrieval Methodology: The satellite and aircraft ultraspectral radiance observation sounding retrieval method uses a "Physical Dual-Regression " method trained to produce accurate retrievals for both clear and cloudy sky conditions. The method relies on using Eigenvector Regression[5,6] "Clear-trained" and "Cloud-trained" retrievals of: surface skin temperature, surface emissivity PC-scores, CO_2 concentration, cloud top altitude, effective cloud optical depth, and atmospheric temperature, moisture, and ozone profiles above the cloud and below thin or scattered cloud (i.e., cloud effective optical depth < 1.5 and a cloud induced temperature profile attenuation < 15 K. The "Clear-trained" regression is a relation relating a "clear sky equivalent" perturbed profile from a clouded radiance spectrum (e.g., an isothermal profile below an opague cloud cover) to the observed radiance spectrum. The "Cloud-trained" regression is a relation relating the true atmospheric profile, both above and below cloud level, to the observed cloud contaminated radiance spectrum.

For the satellite results presented here, the regression relations are derived using 15,000 (NOAA-88, TIGR, ECMWF data set) clear sky soundings uniformly distributed throughout the globe plus 15,000 additional soundings made to be isothermal and saturated below the cloud pressure for each cloud height within each of 8 overlapping cloud height classes: 100-300, 200-400, 300-500, 400 – 600, 500 – 700, 600 – 800, 700-900, and 800-sfc cloud classes. An equal number of unperturbed original and isothermal perturbed soundings provide the representation off any cloud fraction and/or emissivity condition ranging between 0 and 100%. In the satellite radiance regression algorithm development, a cloud radiative transfer model is used to realistically simulate the cloudy radiance spectra used to train the algorithm.

For the NAST-I results presented here, the training data sample used for the dual (clear/cloudy) regression algorithm was taken from a climatological sample of radiosonde data for the JAIVEx region (Gulf Coast). The new algorithm uses regression retrievals obtained from "all-sky" atmospheric condition trained regression coefficients and from radiatively equivalent "clear sky atmospheric condition trained regression coefficients, both for as many as two distinct levels of cloudiness. In all, there are 36 different cloud classification data sets, including clear-sky, the eight single cloud level layers used for the satellite cloud classification as described above, and 28 two level cloud conditions consisting of all combinations of the 8 single level cloud and clear conditions. An equal number of clear sky and opaque overcast cloudy sky condition profiles are included in each cloud classification in order to represent any effective cloud amount condition between 0 (i.e., clear sky) to 100% (an opaque overcast) sky condition. The cloudy sky radiances are computed by setting the temperature profile below the cloud at the cloud temperature and the relative humidity to 100 % for all levels below the assigned cloud top altitude.

The cloud pressure is derived using a cloud classification EOF regression approach. The cloud pressure is predicted using separate regressions for each of the eight cloud categories. The optimal cloud category is chosen as that one whose regression estimate of cloud pressure is closest to the mean for that category. The final value of the "highest possible" cloud-top altitude is assumed to be that altitude below which the "clear-trained" temperature retrieval remains colder than the "cloud-trained" temperature profile and/or or a "forecast" temperature profile, if available. The final profile retrieval is taken as the "clear-trained" solution above the "highest possible" cloud level and the cloud-trained solution below the "highest possible" cloud level. It is noted that the profile below the "highest possible" cloud top is rejected (i.e., declared to be missing) when the maximum difference between the "cloud-trained" and "clear-trained" solution exceeds 15 K. It can be seen from the results presented here that the cloud-altitude stratified dual-regression retrieval procedure alleviates the need for a more time-consuming optimal estimation matrix inversion physical retrieval to account for the non-linearity of the Radiative Transfer Equation (RTE) due to cloud altitude and atmospheric moisture.

II. Ground-based Retrieval Results

Figure 1 shows an example of a time/vertical cross-section of atmospheric thermodynamic structure observed at the NASA Langley Research Center, located in Hampton VA, during the Chemistry And Physics of the Atmospheric Boundary Layer Experiment (CAPABLE). The exact same initial profile is used for all the 3-minute time interval retrievals obtained throughout these two days such that the retrieved time varying vertical structure shown is entirely due to the signatures observed in the 3-minute interval ASSIST radiance spectra. As can be seen, the thermodynamic structure of the lowest 4-km can be retrieved from the AERI/ASSIST spectral radiance measurements with sufficient vertical detail to define the thickness of the PBL and its diurnal variation. The potential temperature defined as that temperature an air parcel would have if it descended adiabatically to the 1000-hPa surface level. A well-developed Planetary Boundary Layer (PBL) is one where the temperature lapse rate within it is near dry adiabatic (i.e., the temperature decreases at a rate of 10 K/km). In this case the potential temperature is nearly constant throughout the PBL

and then increases abruptly with increasing altitude once reaching the top of the PBL. Thus, one can see from figure 1 that the PBL is well developed during the daytime hours and the top of the PBL is near the 2-km level of the atmosphere during the two days shown.

The atmospheric mixing ratio and associated relative humidity retrievals shown also contain sufficient vertical resolution to define detailed PBL moisture characteristics. As can be seen, the mixing ratio within the PBL is nearly constant as characteristic of a well-mixed surface layer. The relative humidity shows a maximum near the top of the PBL (~ 2-km), which often causes the formation of cumulus clouds at the top of the PBL.

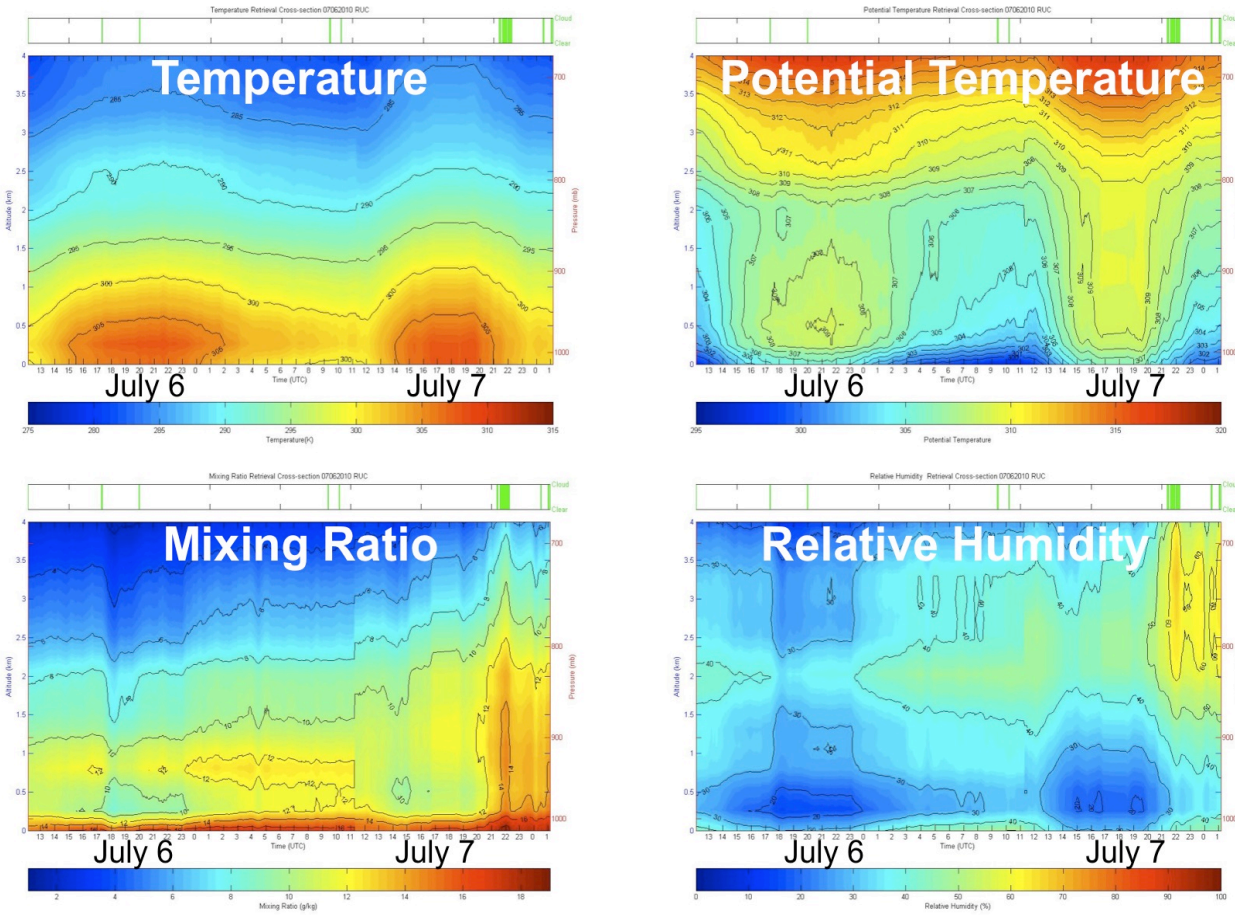

Figure 1. Time cross-section of temperature, potential temperature, water vapor mixing ratio, and relative humidity profiles within the surface to 4-km layer retrieved from ASSIST radiance spectra measured at the NASA Langley Research Center on July 6 and 7, 2010 during the CAPABLE field program.

Figure 2 shows a few example profiles of the tropospheric ozone distribution retrieved from the ground-based spectrometer measurements during the CAPABLE. It can be seen from the comparison of the retrieved profiles with near simultaneous in-situ measurements with ozonesondes and the climatological mean ozone profile, that a polluted PBL can be easily detected relative to a clean PBL using the ground-based spectrometer observations.

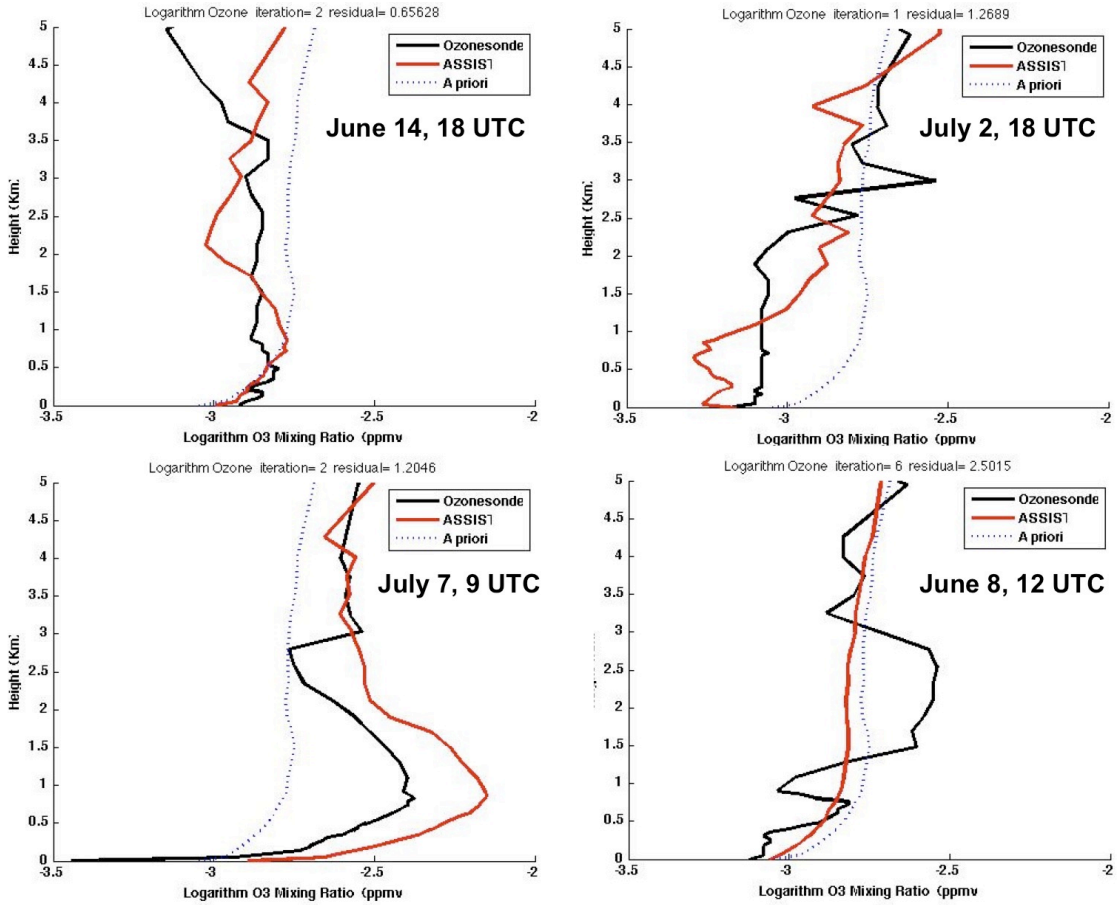

Figure 2. Ozone profiles within the surface to 5-km layer retrieved from ASSIST radiance spectra and ozonesondes observed at the NASA Langley Research Center during July 6 and 7, 2010 during the CAPABLE field program compared to a climatological summer mid-latitude mean ozone profile.

III. JAIVEX

The satellite and aircraft retrieval results shown in this presentation pertain to the Joint Airborne IASI Validation Experiment (JAIVEx)[7] was held during April and May 2007. Seven days of coincident Metop satellite IASI and WB-57 aircraft NAST-I/S-HIS interferometer data were obtained over the DoE ARM CART-site and the Gulf of Mexico. Under flights of the NASA A-train of satellites were conducted on five of the mission days. Coincident dropsondes and remote sensing surface and atmospheric data were provided by the UK BAe-146 aircraft, which under flew the Metop, A-train, and WB-57. The primary sensors on board the WB-57 were the NPOESS Airborne Sounding Testbed - Interferometer (NAST-I)[7] and the Scanning High resolution Interferometer Sounder (S-HIS)[8] and spectrometers. The aircraft base location, dates of the experiment, satellite, airborne, and surface resources being used for JAIVEx, participants, and sponsors in figure 3.

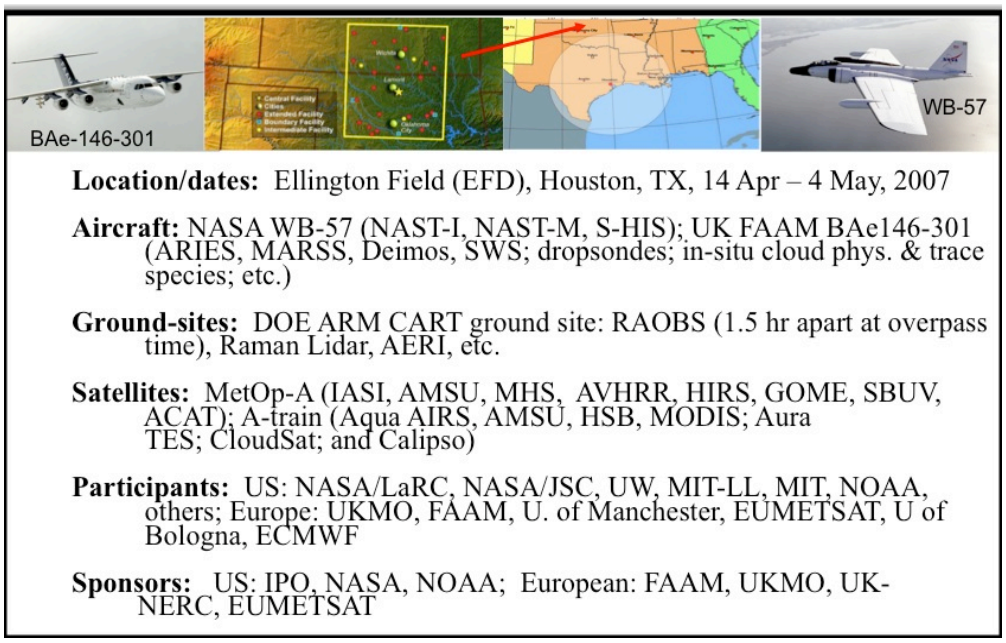

Figure 3: An overview of the JAIVEx resources, participants, and sponsors. A more complete description of the sensors can be found in the publication describing the European AQUA Thermodynamic Experiment[9]

The surface targets of the calibration validation flight missions were the U.S. Department of Energy (DoE) Southern Great Plans (SGP) Atmospheric Radiation Measurement (ARM) facility in north central Oklahoma and the Gulf of Mexico. The ARM facility is well instrumented with in-situ and ground based remote sensors, as desired for meteorological product validation, while the Gulf of Mexico provides a relatively uniform surface background, as desired for spectral radiance measurement validation. One important goal of the JAIVEx was to inter-compare Metop-A operational measurement capability with that provided by the A-train of advanced NASA research satellites.) (The A-train consists of the Aqua, Aura, Parasol, OCO, CALIPSO, and CloudSat satellites). Although the orbits of the Metop and the A-Train are about four hours apart (Metop-A being in a 09:30 descending orbit and the A-train being in a 13:30 ascending orbit), the aircraft missions were of a long enough duration to permit under flights of both the Metop satellite and the A-train. The aircraft sensors were used as a relative calibration transfer reference for each of the satellite systems (e.g., the difference between Metop and aircraft measurements being compared to the difference between A-train and aircraft measurements) in order to account for space and time difference between the measurements from the two satellite systems. This capability was particularly useful for characterizing the differences between the spectral radiance measurements and derived products from the Aqua AIRS and the Metop IASI advanced sounding instruments. Figure 4, below, shows the flight tracks of the WB-57 aircraft during the JAIVEx missions. As can be seen, there were four flights over the ARM-site, 2 daytime and 2 nighttime, and three flights over the Gulf of Mexico, 2 daytime and 1 nighttime. There were a total of five joint Metop and A-train under flights, 3-day time and 2-night time.

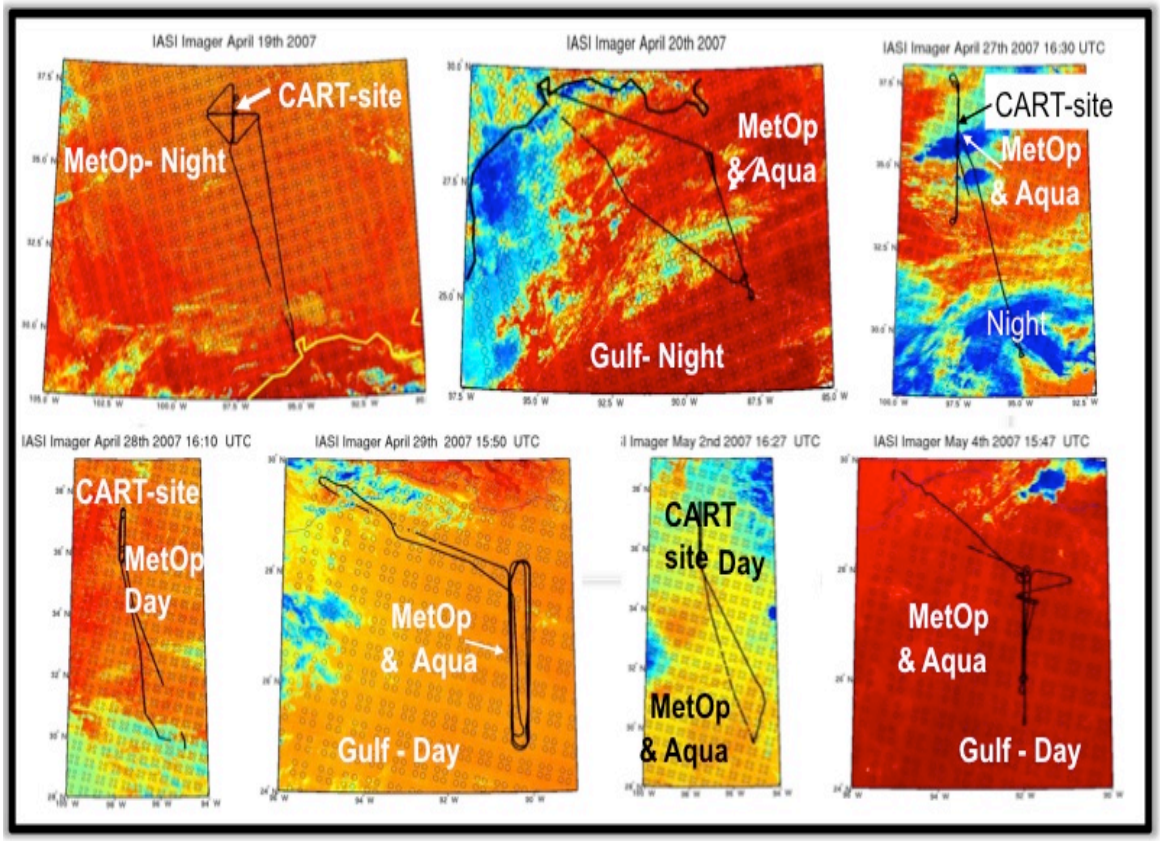

Figure 4. JAIVEx WB-57 flight tracks overlaying an IASI 11 micron image with the IASI sounder footprints shown.

IV Metop Satellite IASI and WB-57 Aircraft NAST-I Retrieval Results

Figure 5 below shows a few examples of retrievals from NAST-I radiance spectra obtained for the JAIVEx region on April 27, 2007 (see upper right hand panel of figure 4). As shown, when there is fairly opaque cloud (e.g., the upper left hand and lower right hand panels of figure 5), there is a large deviation between the "clear-trained" and "cloud-trained" solutions below the cloud with the temperature profiles for the "clear-trained" solution tending towards being isothermal. For such cases, the "cloud-trained" profile below cloud level is regarded as unreliable and therefore missing in the final profile product (black line). For broken or semi-transparent cloud situations (e.g., the upper right hand and lower left hand panels of figure 5), atmospheric profiles can be obtained below cloud level and down to the Earth's surface. For validation of these profile results, atmospheric profiles taken from nearly simultaneous dropsondes are shown (the thick black lines in figure 5). As can be seen, the NAST-I retrievals of temperature are in close agreement with the dropsonde results. For Relative Humidity, there is general agreement and the small-scale differences are believed to be almost entirely due to the different geographical location and vertical resolution of the two measurements. The vertical detail produced by the dual-regression procedure, as applied to the Metop IASI satellite data, is particularly noteworthy.

The next few figures show example IASI retrieval results for the entire JAIVEx region under study. As shown, the cloud pressure altitudes and the cloud mask derived by the dual-regression technique are in very good consistency with the cloudiness depicted by the IASI infrared and the GOES visible imagery. It can also be seen that a very large portion of this scene is composed of a very high dense cloud cover with some cirrus and lower broken cloud cover around the edges of the high altitude dense clouds. This cloud condition provides a very strong challenge to obtaining accurate atmospheric profiles remotely from satellite or aircraft infrared spectral radiance data for this particular day of the JAIVEx. The white patches shown in this figure, and subsequent figure, are at locations where the IASI radiance spectra were flagged to be unreliable.

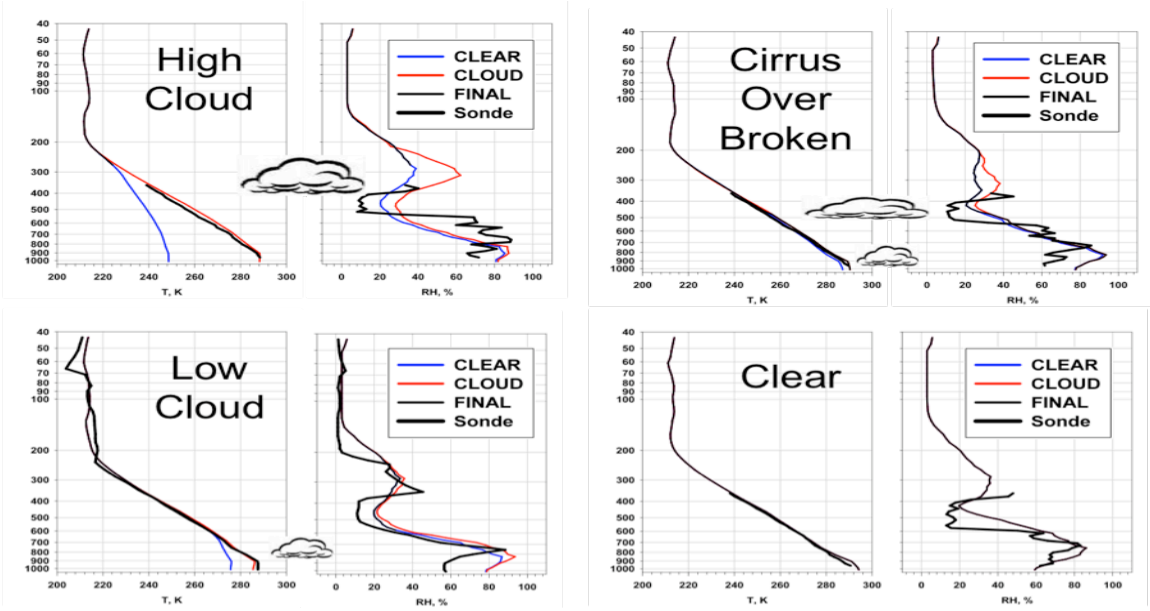

Figure 5. A few examples of "clear-trained", "cloud-trained", and "Final" retrievals obtained from the WB-57 aircraft NAST-I spectra on April 27, 2007. The thin black line displays the "final" NAST-I produced dual-regression retrieval. The thick black line displays a nearby dropsonde observation.

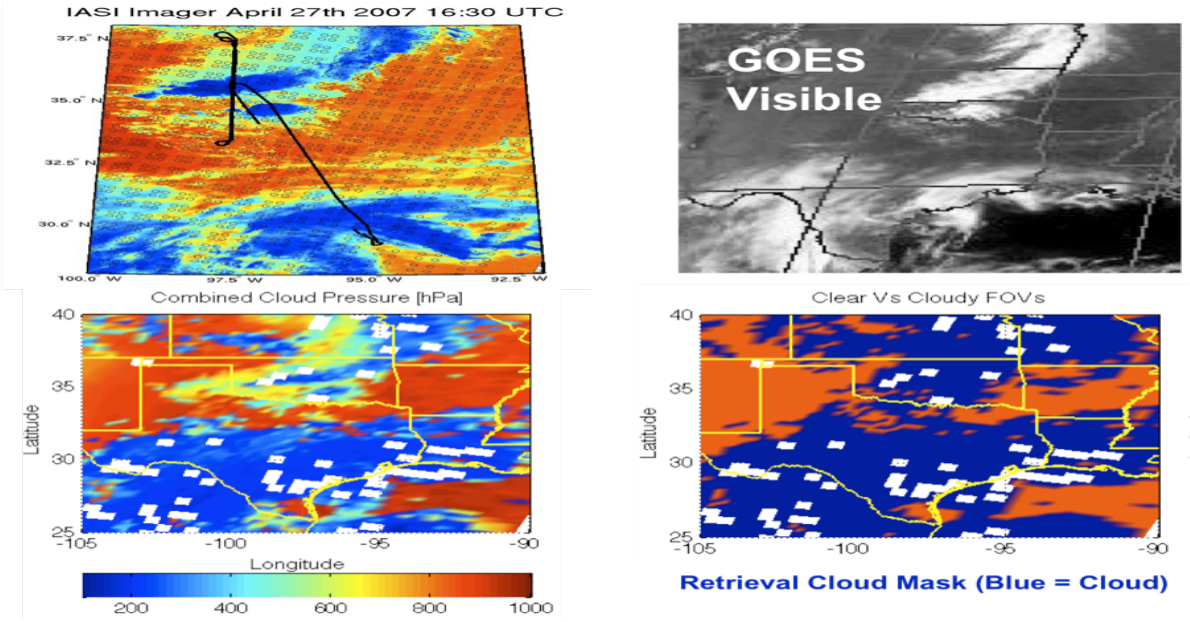

Figure 6. Cloud height and cloud mask results obtained using the dual-regression with Metop IASI measurements obtained on April 27, 2007. The cloudiness observed with the IASI infrared imager and the GOES visible imager is shown for comparison.

Figures 7 shows the surface parameters derived from IASI radiance spectra while figures 8-10 show results obtained for the 850-hPa, 500-hPa, and 100-hPa atmospheric levels. As can be seen there is good overall agreement between the dual regression IASI retrievals and the ECMWF analyses, the major difference being attributed to the different spatial resolutions of the two sets of data. One can see that the density of IASI retrievals increases, as expected, as one goes to higher levels, the coverage becoming complete at the 100-hPa

level, which is above all the clouds in this region. Unfortunately, the cloud cover is generally high and dense for this case so that there is a large amount of missing data. Despite the large amount of missing satellite data due to the dense cloud cover, the right hand panels of figures 8-10 show that the satellite ultraspectral data serve to add significant spatially coherent mesoscale atmospheric structure to the ECMWF analyses.

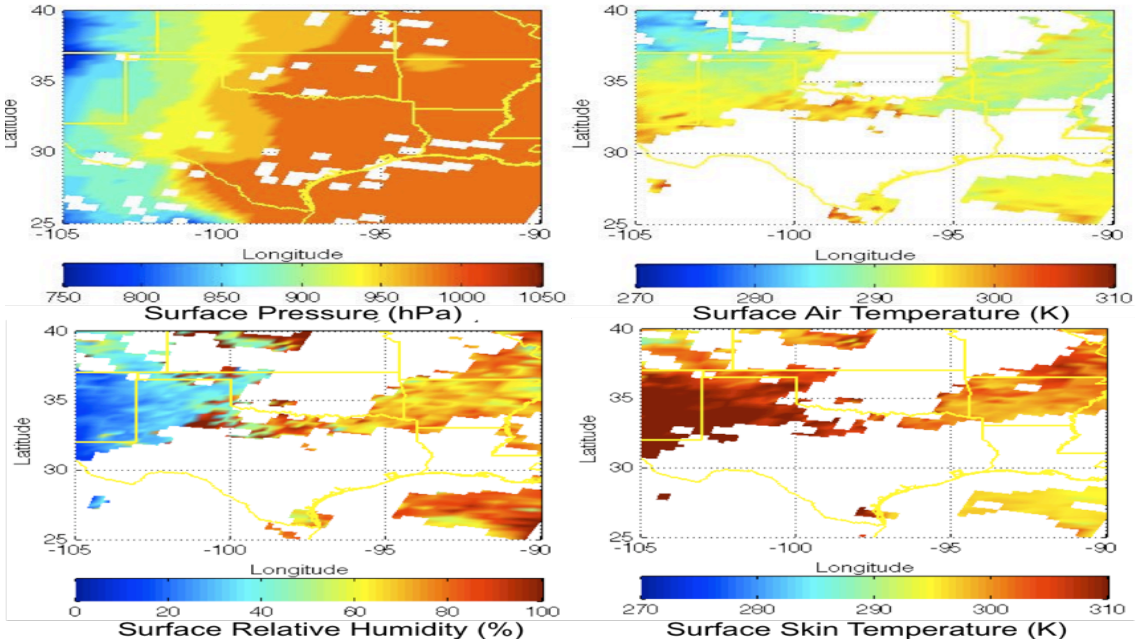

Figure 7. Surface pressure, air temperature, relative humidity, and surface-skin temperature retrieved from IASI data for April 27, 2007.

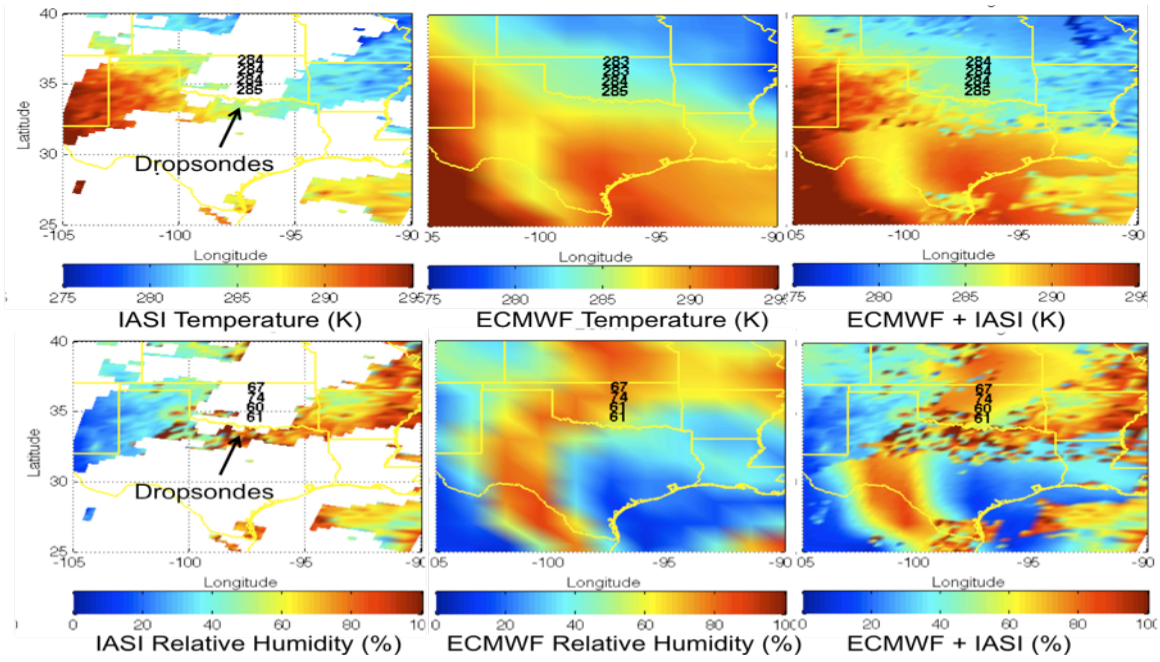

Figure 8. The temperature and relative humidity retrieved at the 850-hPa level from IASI data for April 27, 2007. The ECMWF analyses and dropsonde measurements from the BAe-146 aircraft are shown for comparison. The right hand panels show the combination of the IASI retrievals and the ECMWF analyses.

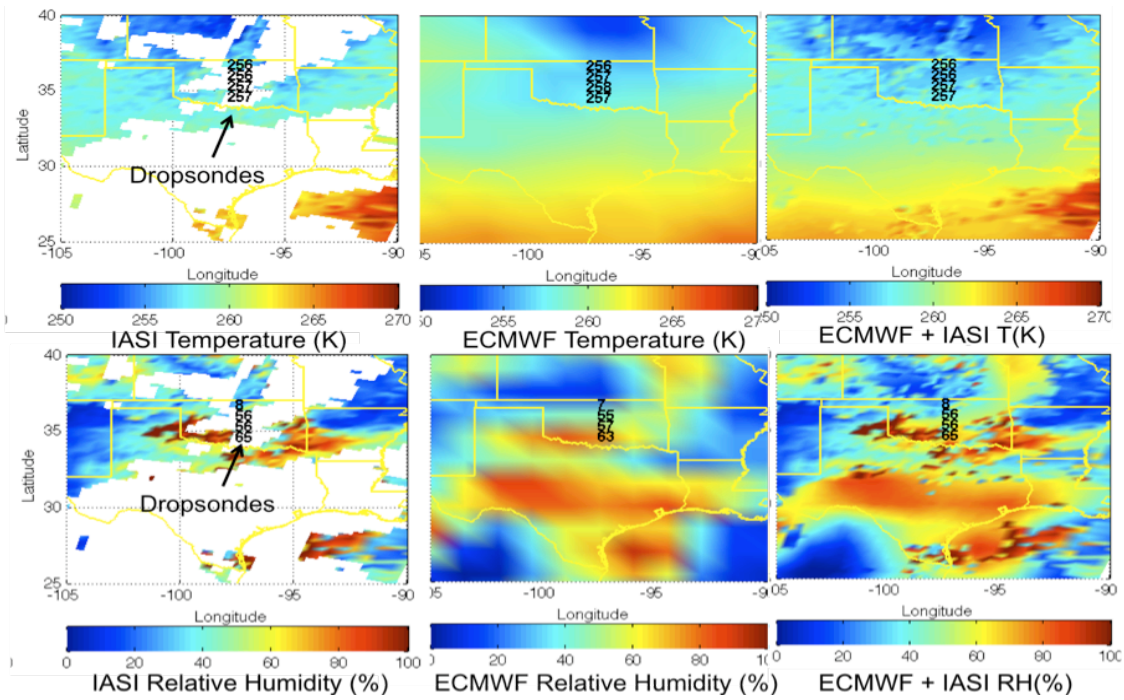

Figure 9. The temperature and relative humidity retrieved at the 500-hPa level from IASI data for April 27, 2007. The ECMWF analyses and dropsonde measurements from the BAe-146 aircraft are shown for comparison. The right hand panels show the combination of the IASI retrievals and the ECMWF analyses.

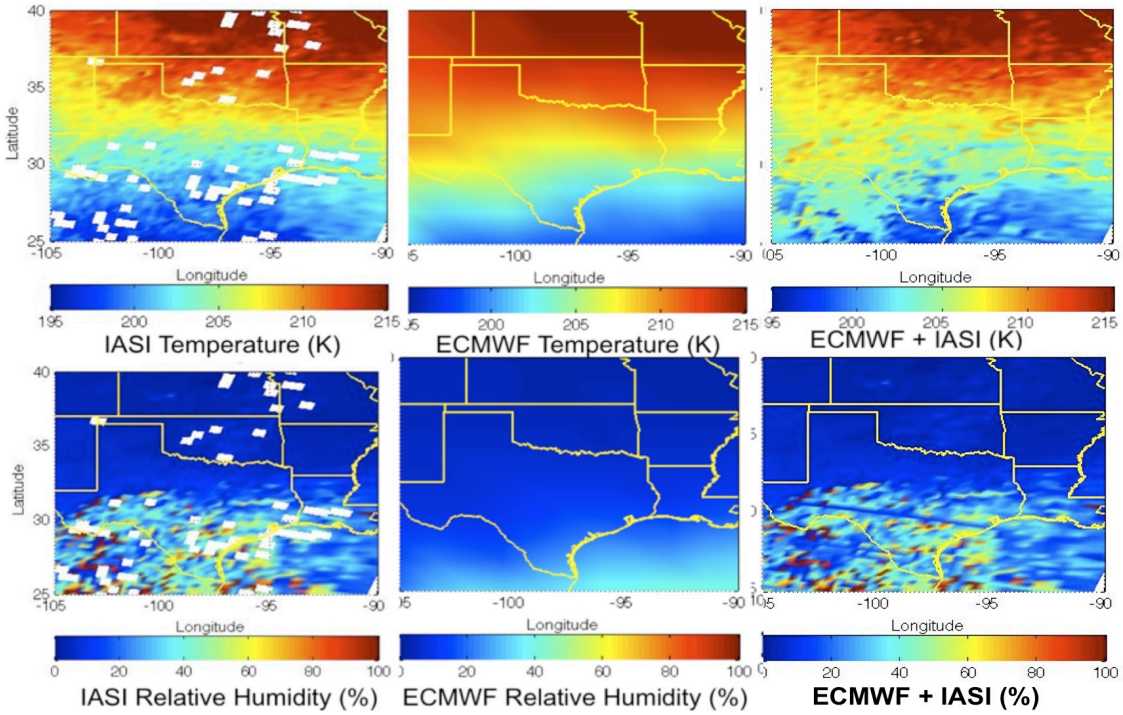

Figure 10. The temperature and relative humidity retrieved at the 100-hPa level from IASI data for April 27, 2007. The ECMWF analysis is shown for comparison. The right hand panels show the combination of the IASI retrievals and the ECMWF analyses.

Figure 11 shows the standard deviation and the mean differences between the IASI retrievals and the ECMWF analysis profiles at the IASI retrieval locations. It is believed that most of the difference shown is due to the spatial resolution of the soundings rather than to errors in the IASI retrieved atmospheric profiles. The yield of IASI soundings shows the abrupt decrease in coverage at the lower atmospheric levels due to the increasing probability of encountering opaque clouds.

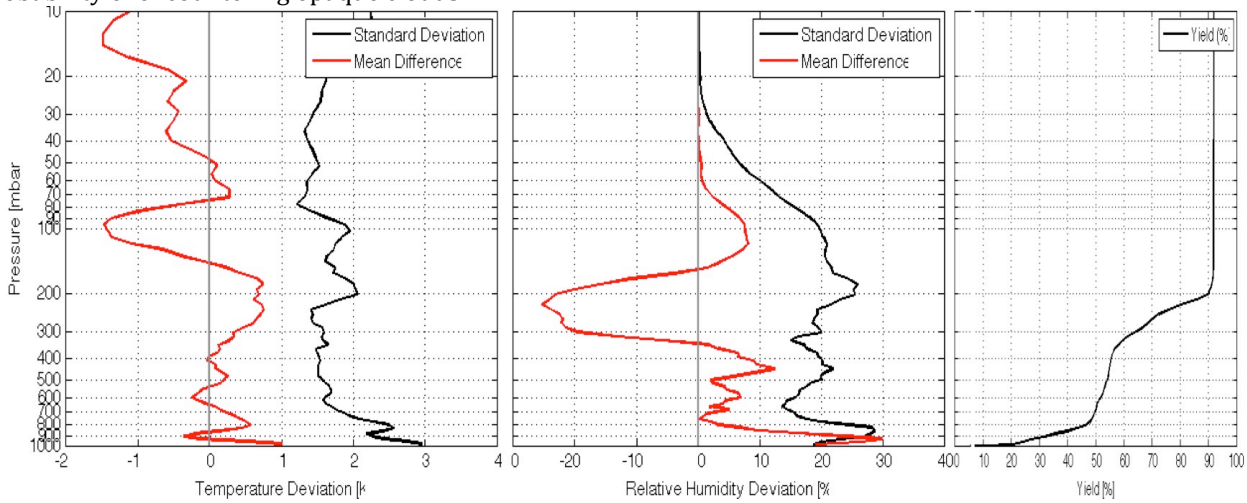

Figure 11. Standard deviation and mean difference between the IASI retrievals and the ECMWF analysis profiles at the IASI retrieval locations. The yield of IASI soundings is shown in the right hand panel.

Figure 12 shows comparison of NAST-I aircraft, IASI, and ECMWF profiles with the ARM-CART-site radiosonde released at the time of the IASI overpass. The NAST-I and the IASI profiles shown were chosen to be those, which reached the ground level, closest in time and distance from the ARM-site radiosonde observation. For the 2-km horizontal resolution NAST-I, the distance from the ARM-site is only 4-km compared to the 50-km distance of the 12-km horizontal resolution IASI profile. As can be seen the relative accuracy of all of these profiles is appears to be comparable with the highest horizontal resolution and geographically closest to the ARM-site NAST-I retrieval showing the best agreement with the radiosonde observation.

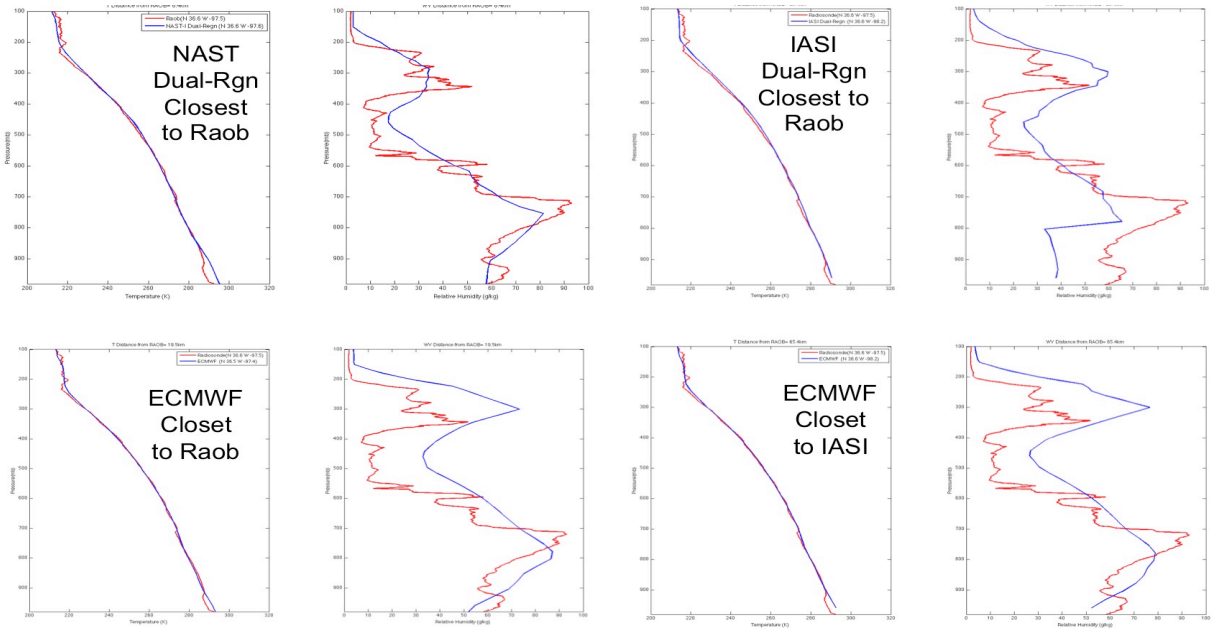

Figure 12. Comparison of NAST-I aircraft, IASI, and ECMWF profiles with the ARM-CART-site radiosonde released at the time of the IASI overpass. released at the time of the IASI overpass.

V SUMMARY AND CONCLUSIONS

Significant advances in profiling the fine scale thermodynamic structure of the atmosphere are resulting from satellite, airborne, and surface-based high-resolution radiance spectra. Satellite observations provide mesoscale spatial structure not resolved by conventional radiosonde observations. Ground-based observations provide temporal resolution not provided by conventional radiosonde observations. Significant progress is being made in profiling the boundary layer structure of certain greenhouse and pollutant gases. Climate quality soundings will be obtained by combining satellite radiance measurements with ground-based radiance measurements for the retrieval of the atmospheric profiles.

VI REFERENCES

[1] Smith Sr., W. L., Revercomb, H., Bingham, G., Larar, A., Huang, H., Zhou, D., Li, J., Liu, X., and Kireev, S., "Evolution, current capabilities, and future advances in satellite ultra-spectral IR sounding", Atmos. Chem. Phys. Discuss., 9, 6541-6569, (2009).

[2] Knuteson, R. O.; Revercomb, H. E.; Best, F. A.; Ciganovich, N. C.; Dedecker, R. G.; Dirkx, T. P.; Ellington, S. C.; Feltz, W. F.; Garcia, R. K.; Howell, H. B.; Smith, W. L.; Short, J. F. and Tobin, D. C., "Atmospheric Emitted Radiance Interferometer, Part I: Instrument design". Journal of Atmospheric and Oceanic Technology, 21, 12, .1763-1776 (2004).

[3] Knuteson, R. O.; Revercomb, H. E.; Best, F. A.; Ciganovich, N. C.; Dedecker, R. G.; Dirkx, T. P.; Ellington, S. C.; Feltz, W. F.; Garcia, R. K.; Howell, H. B.; Smith, W. L.; Short, J. F. and Tobin, D. C.. Atmospheric Emitted Radiance Interferometer, Part II: Instrument performance", Journal of Atmospheric and Oceanic Technology, 21, 12, 1777-1789 (2004)

[4] Rochette, L William L. Smith, Michael Howard, and Tim Bratcher, "ASSIST, Atmospheric Sounder Spectrometer for Infrared Spectral Technology: latest development and improvement in the atmospheric sounding technology", oc. SPIE 7457, 745702 (2009).

[5] Smith, W. L.; Zhou, D. K.; Huang, H.-L.; Li, Jun; Liu, X. and Larar, A. M., "Extraction of profile information from cloud contaminated radiances. ECMWF Workshop on Assimilation of High Spectral Resolution Sounders in NWP", Reading, UK, 28 June-1 July 2004. ECMWF Workshop Proceedings. European Centre for Medium-range Weather Forecasts (ECMWF), Reading, UK, 145-154 (2004)

[6] Smith, W. L., D. K. Zhou, A. M. Larar, S. A. Mango, H. B. Knuteson, H. E. Revercomb, and W. L. Smith Jr., "The NPOESS Airborne Testbed Interferometer – Remotely Sensed Surface and Atmospheric Conditions during CLAMS" , J. Atmos. Sci., 62, 1118 – 1134 (2005).

[7] Smith, W., Larar, A., Taylor, J., Revercomb, H., Kireev, S., Zhou, D., Liu, X., Tobin, D., Newman, S., Schlüssel, P., Clough, A., Mango, S., and St. Germain, K., "Joint Airborne IASI Validation Experiment (JAIVEx) - An overview", Proc. Int. ATOVS Study Conf. XVI, Angra dos Reis, Brazil, CIMSS, University of Wisconsin–Madison, (2008).

[8] Revercomb, Henry E.; Tobin, David C.; Knuteson, Robert O.; Best, Fred A.; Smith, William L.; van Delst, Paul; LaPorte, Daniel D.; Ellington, Scott D.; Werner, Mark W.; Dedecker, Ralph G.; Garcia, Ray K.; Ciganovich, Nick K.; Howell, H. Benjamin; Dutcher, Steven and Taylor, Joe K., "Validation of Atmospheric InfraRed Sounder (AIRS) spectral radiances with the Scanning High-resolution Interferometer Sounder (S-HIS) aircraft instrument", International TOVS Study Conference, 13th, Sainte-Adele, Quebec, Canada, (2003).

[9] Taylor, J. P.; Smith, W. L.; Guomo, V.; Larar, A. M.; Zhou, D. K.; Serio, C.; Maestri, T.; Rizzi, R.; Newman, S.; Antonelli, P.; Mango, S.; Di Girolamo, P.; Esposito, F.; Grieco, G.; Summa, D.; Restieri, R.; Masiello, G.; Romano, F.; Pappalardo, G.; Pavese, G.; Mona, L.; Amodeo, A. and Pisani, G.. EAQUATE, "An international experiment for hyperspectral atmospheric sounding validation.",Bulletin of the American Meteorological Society, 89, 2, 203-218 (2008).

VII Acknowledgements

The authors acknowledge the financial support of NASA, NOAA, and the DOE for their support of this research. The support of Michael Howard (NSTech) and Luc Rochette (LRTech) in acquiring the CAPABLE ASSIST data is gratefully acknowledged.